Nov. 2012 Renewal Proposal for RD2012-14

to Develop Calorimeters for EIC

The EIC Calorimeter R&D Consortium

– Contact Persons: H.Z. Huang huang@physics.ucla.edu and C. Woody woody@bnl.gov

E. Kistenev, S. Stoll, A. Sukhanov and C. Woody

(PHENIX Group, Physics Department)

E. Aschenauer and S. Fazio

(Spin and EIC Group, Physics Department)

Y. Fisyak

(STAR Group, Physics Department)

Brookhaven National Laboratory

W. Jacobs, G. Visser and S. Wissink

Indiana University

S. Heppelmann

Pennsylvania State University

C. Gagliardi

Texas A&M University

L. Dunkelberger, H. Z. Huang, G. Igo, K. Landry, S. Trentalange, O. Tsai and Q. Zhang
University of California at Los Angeles

Y. Zhang, H. Chen, C. Li and Z. Tang

University of Science and Technology of China

1) *Introduction*

Within the EIC calorimeter consortium, there are four major R&D efforts to develop calorimeter technology: 1) the RD1 (2011) effort to develop a W-powder/Scintillating Fiber-based compact SPACal-type electromagnetic calorimeter (EMC); 2) the development of a Tungsten plate-based accordion-shaped EMC; 3) the R&D project on crystal calorimeter development based on BSO and PWO crystals; and 4) Monte Carlo simulations for both detector design and physics to develop detector requirement specifications and physics capabilities for a comprehensive detector at EIC.

At the last EIC detector R&D review meeting in May 2012, the RD1 proposal was partially funded to address several issues and questions raised by the committee. In this renewal proposal we will provide a report on our progress and answers to questions that we can address with the information and technical data that we have. Some more general questions, in particular, EIC machine development related questions will take much longer time and a broader group to address. We also propose to focus our hardware related issues in the coming year for the EMC development. The goal of R&D in Year Two is to extend the W powder Sc/Fi technique: to build wedge-type towers, develop compact readout, and test it with the beam (targeted energy resolution ~10%/√E). This R&D should give us good idea of the limitations of the W/ScFi technique for applications in the central region. At the same time, questions of projectivity and granularity will be investigated with simulations.

The project for the development of an accordion-shaped tungsten plate EMC was fully funded in May 2012. We will provide a brief progress report on this effort.

The crystal R&D project was funded in the fall of 2011. The USTC group has been working closely with the SICCAS to produce prototype BSO and PWO crystals. Several samples have been tested at the USTC lab. We will report some testing results and outline our plan for the near future.

The simulation effort involving tracking, calorimeter subsystems and the physics Monte Carlo is a major task undertaken by the BNL EIC/Spin group. Joint phone meetings and face-to-face meetings have been held among the tracking and calorimeter consortia. The overall physics performance depends on both the sub-system performance and the optimization of the detector configuration. This will be a multi-year effort with continued collaboration among the physics simulation groups and the hardware R&D groups. We are working towards a baseline detector configuration so that detailed sub-system requirements can be developed through physics simulations. System integration issues, calibration and monitoring requirements will also be investigated through the Monte Carlo effort. We expect to report our progress on this front at the review meeting in Dec. 2012.

The Indiana Group (S. Wissink, W. Jacobs and G. Visser) has joined the EIC calorimeter consortium. The IU group was responsible for the construction and operation of the STAR Endcap EMC. The group has been a leading spin physics group in the STAR collaboration. They will participate in the EIC calorimeter R&D project with a near-term emphasis on the electronics read-out development.

The STAR Group at BNL (Y. Fisyak) has also joined our effort. Y. Fisyak has been working on the neutron radiation dosage in the STAR detector environment. He will continue to help us to address the radiation issue at EIC in the coming years.

2) *Renewal Proposal for RD1 – W-Powder/Scintillating Fiber SPACAL Development*

2.1 Overview

The last proposal from the RD1 team was reviewed at the May 2012 meeting and was partially funded. The committee asked us to address several issues related to the prototype EMC modules and questions related to the test beam results. Here we give a brief report on the progress that we have made since last May in response to the committee comments. We propose to continue our momentum in the EIC calorimeter development. Our main emphasis in the next year will be to focus on the light collection scheme and the development of a compact read-out system and extend the W-powder/ScFi EMC construction technology to a Barrel calorimeter application. The addition of new groups in the calorimeter consortium (IU, BNL-STAR) brought much needed expertise in neutron background calculations, spin physics, technical know-how in construction and operation of large calorimeters, and electronics read-out technology for SiPMs.

2.2 Mechanical Properties.

The homogeneity of the W/ScFi matrix is important for the uniform response of the detector. The influence of different non-uniformities on the energy resolution of the calorimeter will be discussed in the instrumental effect section. Here we address the question from the review committee about mechanical properties of the prototypes that we built in 2011.

The mechanical properties of the W/ScFi composition of the prototypes constructed during the first year of the R&D were studied prior the test run. The 'differential' and 'integral' non-uniformities were measured by slicing pre-production samples along their length after the final assembly of the super-modules. The 'differential' non-uniformity (density) was measured to be less than 1%. The 'integral' non-uniformity was found to be close to 0.5%. The weights of the super-modules are 4567, 4651, 4627, and 4630 g., where the smaller mass of the very first super module is due to a thicker layer of Epoxy/Fibers mixture at the front of the block. For the rest of the super modules the process of forming this layer was changed.

The tolerances on external dimensions of the super modules are close to 50 μm. They are defined by the precision photo-etched meshes which hold the fibers in place, by the tolerances of the molding form, the quality of machining of individual sub-assemblies, and by the gluing of super modules from two sub-assembly units. The tolerances of the meshes are close to 15 μm on external dimensions and positions of the center of the holes. The tolerance on the diameter of the holes is 30 μm.

To our knowledge there are no published data on 'differential' and 'integral' non-uniformities of the ScFi type calorimeters, as presented above. The mechanical tolerances for individual components, for example, for thickness of the lead sheets and dimensions of the grooves for the fibers from the H1 calorimeter, are approximately at the same level as in our design. The tolerance for the width was 100 μm.

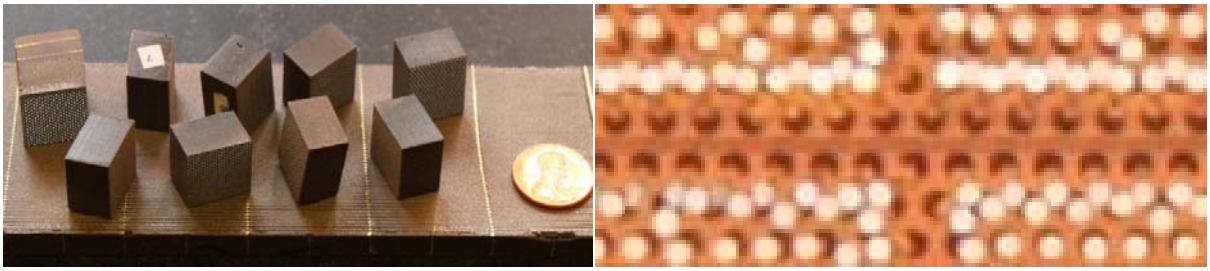

Figure 2.1: (Left): Samples of the W/ScFi prototypes which were used to measure uniformity of the W/ScFi composition. (Right): Cropped image of the central part of the super-module showing that the positioning of the fibers was carefully preserved during the gluing of the super-modules from two sub-assemblies. The glue joint is horizontal line at the middle of the photograph.

Some mechanical properties of the W/ScFi mixture were measured during summer 2012. The Young, Shear and Bulk moduli are measured to be 200 GPa, 75 GPa and 243 GPa respectively. These values are close to the same parameters for structural steel and about factor of 15 higher than Lead, which is normally used in Sc/Fi calorimeters. The strength of the W/ScFi composition has significant advantage for mechanical design of the detectors. These numbers were used to estimates stresses and deflections of a stack of about 2 meters high (the approximate size of a possible forward calorimeter system for EIC to measure outgoing hadrons). Due to the high stiffness of the material, the sag of the whole stack is estimated to be about 1.5 μm. The small distortion indicates that with such a structure the scintillation fibers will not be damaged at the bottom of the stack. Future work in this direction will be required. In particular, light output and long-term effects under loading will be studied as well as a complete set of measurements of mechanical properties of the W/ScFi mixture (yield strength, ultimate strength etc.).

To summarize: mechanical tolerances and uniformity in the prototypes tested at FNAL is at least at the same level as one of the best ScFi calorimeters used in the past. The homogeneity of the prototypes is 1% differential and 0.5% integral which we cannot compare with the traditional techniques due to the lack of data. It is sufficiently good for high resolution EIC sampling calorimeters. The mechanical properties of the W/ScFi modules from our R&D prototypes are much better than those of traditional Lead/Fiber structures when constructing a large size calorimeter.

2.3 Radiation Tolerances and Neutron Fluence

The radiation dosage for the detectors at EIC will have contributions from the machine-related background sources and physics collisions. We will first address the physics collision-related background since the machine-related background depends on details of the machine design and performance which have not been completely settled. The question of beam-induced background was discussed during a recent EIC simulation workshop. For the eRHIC design, the power and spectral distribution of synchrotron radiation for both ARCs and IRs were calculated. For example, in the IP region at eRHIC, the SR line power density is about 50 mW/mm, compared to50 kW/mm at HERA, after the upgrade. The neutron flux generated by SR in the Al vacuum chamber through photonuclear reactions is negligibly small (~10^{-6} n/sec). For the first stage of eRHIC (5-10 GeV), the aluminum vacuum chamber is capable of preventing SR photons from escaping. For higher energies, additional shielding may be required. A more complete study of SR in the IP will be continued by the CAD group.

To estimate the radiation level for EIC detectors due to collision products alone we scale results for pp collisions (report of the task group on radiation levels in the SSC interaction region [1], new dose calculations for LHC detectors [2]). The calorimeter is assumed to be a hollow lead sphere with an internal radius of 2 meters with forward and backward cones at $\eta > 6$ removed [2].The integrated luminosity per year was taken to be 10^{41} cm^{-2} and the cross section for ep collisions $\sigma_{ep} = 0.060$ mb. Under these assumptions, the direct scaling of results of total dose (Table 4 [2]) gives a radiation dose in the rapidity interval 0-1 to be 45 rad, and in the rapidity interval 4-5 to be 170 krad per year. These are small dose levels. For example, when ScFi technology was proposed for LHC, the effect of radiation damage was studied for a SPACAL type detector. The conclusion of these studies was that the maximum allowable dose was 6.1 Mrad (criteria are: degradation of EM energy resolution 0.8%, nonlinearity for electrons 2.5% due to radiation damage) [3].

In general, the topic of radiation damage in scintillation fibers is very complex (similar to wire aging in gaseous detectors). One has to take into account multiple factors; total dose and dose rate, ambient temperature during irradiation, annealing effects, coloration of the basic matrix, chemical structure and molar fractions of the added dopants, surrounding media (type of gas, epoxy etc), polymerization time during production, oxygen content in fibers etc. Major changes in the fibers due to radiation include: formation of color centers in the core which lead to a decrease in the attenuation length, chemical degradation of dopants which lead to a reduction of absolute light yield and finally degradation of the cladding layers which again leads to a decrease in the attenuation length due to decreased reflectivity between core and clad layers. Because of the complexity of the problem, the data on radiation hardness for scintillation fibers from available literature vary significantly. Reports vary from seeing significant degradation at a level of 10 krad to almost no degradation at the 1 Mrad level. Later, in the instrumentation effects section, we come back to this question again. At this stage of the R&D we do not expect the radiation hardness to be a critical issue. It is absolutely clear that in thefuture with more accurate dose estimate (including one coming from the machine background) we will have to address this question again with our own testing data.

To estimate possible neutron fluxes we again look at pp results (RHIC, pp 510 GeV). The scaling factor for ep is approximately 0.1. This factor comes from difference in interaction rate and colliding species (rates, ep < 600 kHz, compared to 2 MHz for pp 510 GeV, with the proton beam being the main source of the neutrons). With such an approach, a crude estimate of the neutron flux for top energy ep collisions with an integrated luminosity of 10^{41} cm^{-2} is ~10^{10} cm^{-2} at R= 7.5 cm at mid rapidity and at R=30 cm @ Z=8 m (forward rapidity up to ~5 for outgoing protons). As a reference we took the STAR interaction region configuration at RHIC (region of +- 20 meters from the IP). An accurate description of the geometry in simulation of the neutron fluxes is very important. For example, details like the inclusion of cooling water, electronics racks at the platforms and an accurate description of the concrete in ceilings, walls and floors in the experimental hall changes the distribution of the neutron production vertices, as well as their energy spectra. Examples are given in figures 2.2 and 2.3, below (the top figure does not model the cooling water in the solenoidal magnet and is missing many components on the electronics platforms, and the overall statistics are also smaller).

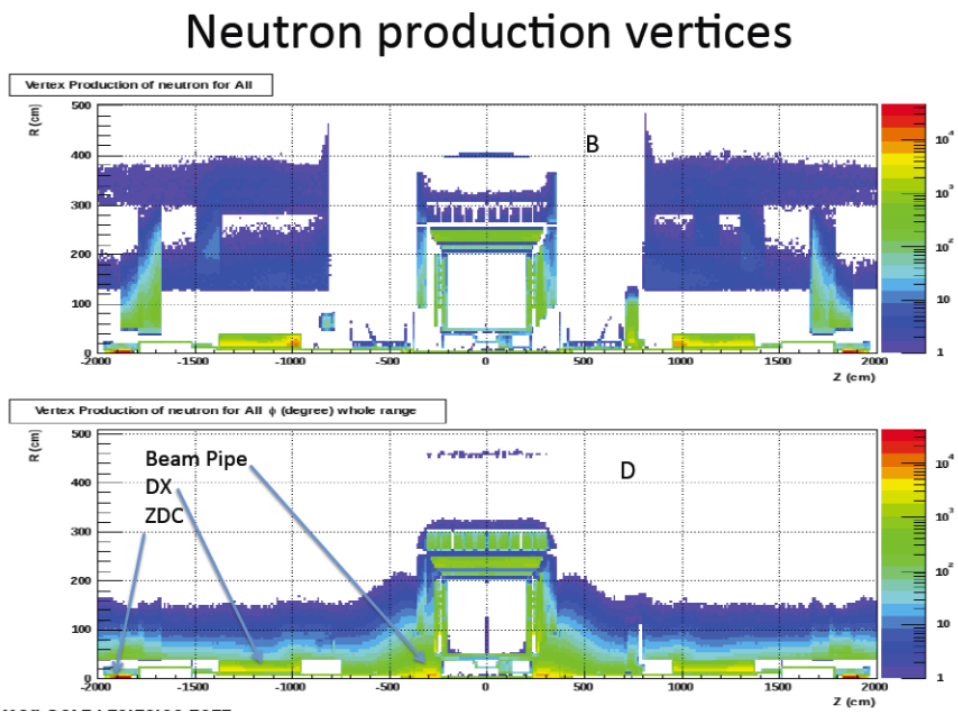

Figure 2.2: Neutron production vertices for STAR 510 GeV pp.

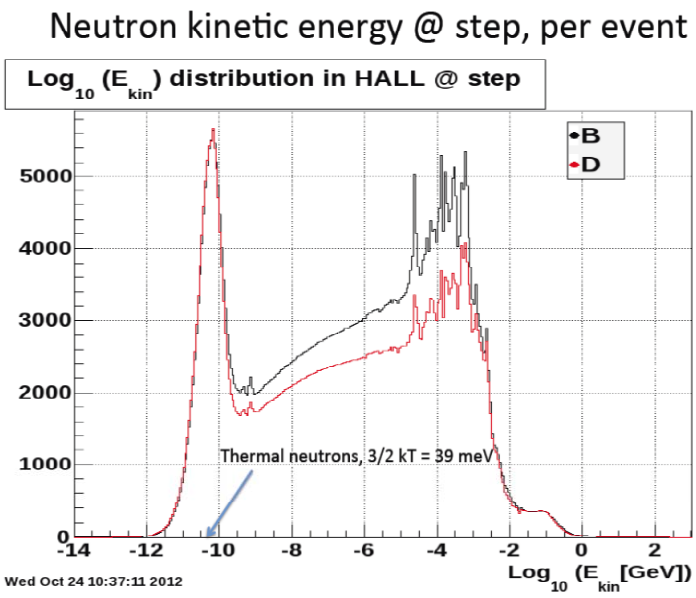

Figure 2.3: Energy spectrum of neutrons depending on the different geometries described in the text.

The main source of the neutrons at STAR is 'machine' related background: beam pipe, DX magnet and zero-degree calorimeter. Obviously the design of the IP IR for EIC will be different from that of STAR, as well as the EIC detector itself and the experimental area. Thus, any scaling should be taken with

caution. Calculations with realistic geometry of the EIC experimental setup will be required to obtain more accurate result. At this time, we believe that neutron fluxes at eRHIC will not exceed 10^{10} n/cm^{-2} (for an integrated luminosity of 10^{41} cm^{-2}).

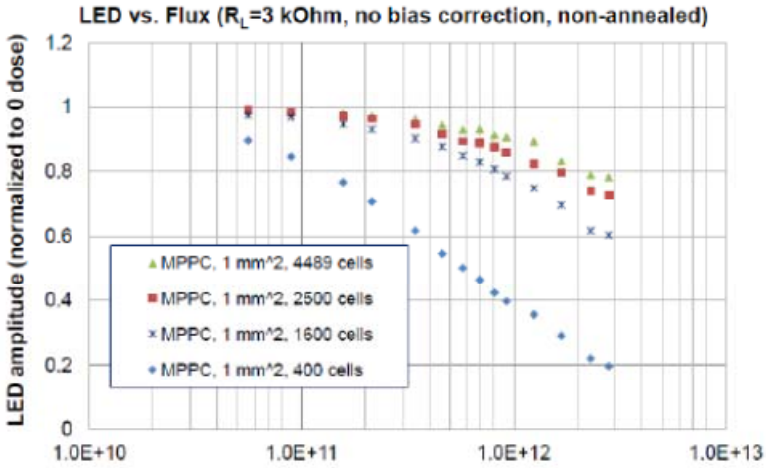

Figure 2.4: Change of the gain of Hamamatsu MPPC after irradiation with neutrons [4].

For readout of the EIC sampling calorimeters (barrel, forward end cap) we want to investigate SiPMs or, as an alternative, large area APDs. However, the experience of CMS with anomalous signals in their calorimeters lead to some concerns about the application of APDs to scintillation fiber calorimeters. The obvious concern is for neutron damage in any Si-based devices. The latest generation of SiPMs presently is under intensive testing for detector upgrades in the near future at the LHC. In particular, both CMS and ATLAS are planning to replace their HPDs with SiPMs. The requirements for the CMS SiPMs are the ability to work with neutron fluxes up to $2*10^{12}$ n/cm^{-2} (leakage current < 200 uA, fraction gain x PDE > 65%). The latest HAMAMATSU MPPC with a 15 um pixel size already satisfies these requirements as shown in figure 2.4 and figure 2.5.

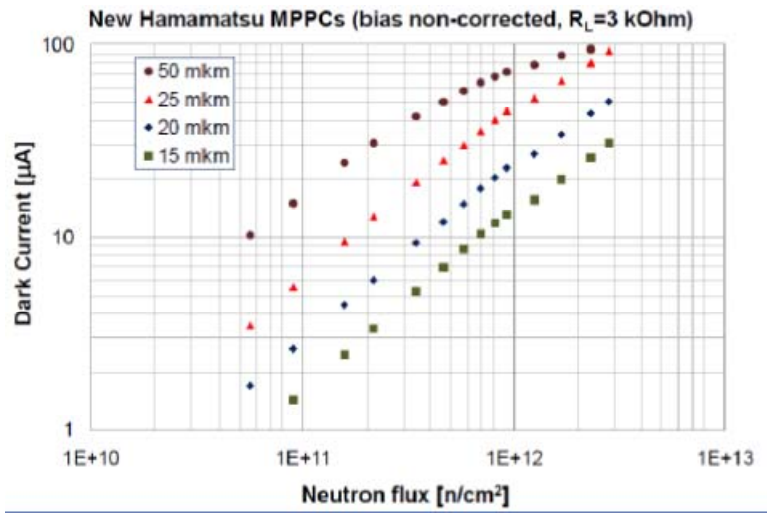

Figure 2.5: Leakage current after irradiation with neutrons [4].

To summarize, an exact calculation of neutron fluxes will require detailed information about the designs of the IP (machine elements, beam pipe etc.), EIC detector, experimental hall, etc. A preliminary estimate of the neutron flux for top energy ep collisions at EIC are 10^{10} cm^{-2} for an integrated luminosity of 10^{41} cm^{-2}. This level of neutron flux does not pose a challenge for calorimeter readouts based on SiPMs.

2.4 Discussion of Test Run Results

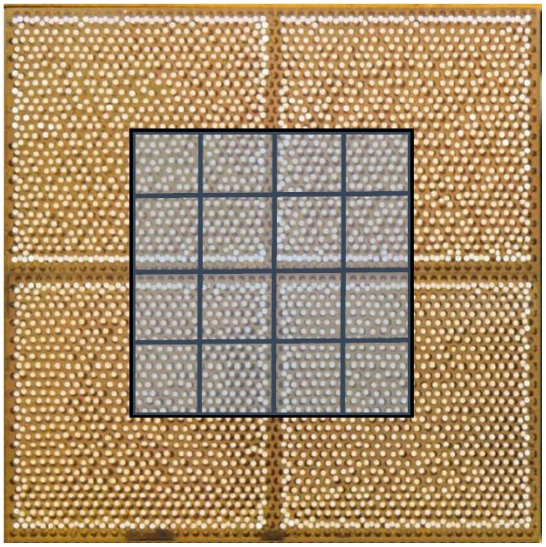

Figure 2.6: Sketch of beam impact area (light blue) used to measure energy resolution of the SPACAL. The brown square is 5.3 x 5.3 cm^2 and the light blue square is 2 x 2 cm^2.

To measure the energy resolution of the calorimeters we allowed a wide impact area in order to sample mechanically different parts of the detector, as shown in figure 2.6. The size of the super module is 5.3 x 5.3 cm^2. The light blue grid shows the approximate binning possible with the scintillating hodoscope, where each bin is 4.8 x 4.8 mm^2. Due to the large width of the test run beam, the energy resolution derived for these impact points was almost uniformly distributed over the entire area of 2 x 2 cm^2 shown in light blue in the middle of the super-module. Thus any transverse non-uniformity that could influence the energy resolution is automatically included in our measured energy resolution. The only correction made to the measurements is for beam momentum spread which was estimated with a "standard" lead glass calorimeter provided to us by FNAL. This correction is rather small for low beam momentum settings ($\Delta p/p$ ~2.7% at 1-4 GeV, 2.3% at 8 GeV), but it becomes the dominant factor at higher energies. We attempted to take data at 16 and 32 GeV but found that it is impossible to estimate the momentum spread of the beam at these settings due to backside leakage in the standard lead glass calorimeter (understanding of the beam conditions and beam tunings took ~50% of the test beam time). Thus, we dropped any attempt to measure the response of the prototypes at energies above 8 GeV.

The resolution of prototypes with different configurations is shown in figure 2.7. The "proof-of-principle", which was the goal of the first year of R&D, is demonstrated in the comparison of the SPACAL resolution with the GEANT4 prediction, shown as a dotted line.

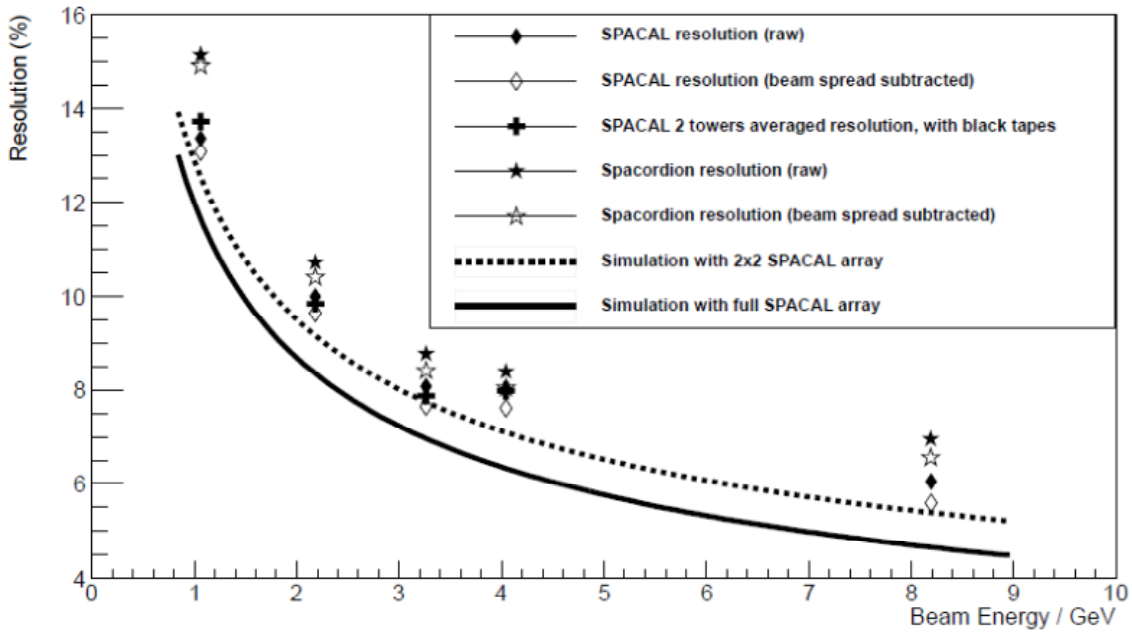

Figure 2.7: SPACAL and SPACORDION energy resolutions as measured in the FNAL test run and compared with GEANT4 predictions. Impact points were restricted to a 2x2 cm^2 square at the center of the super-module. Data are from the EIC R&D Year 1 test beam results.

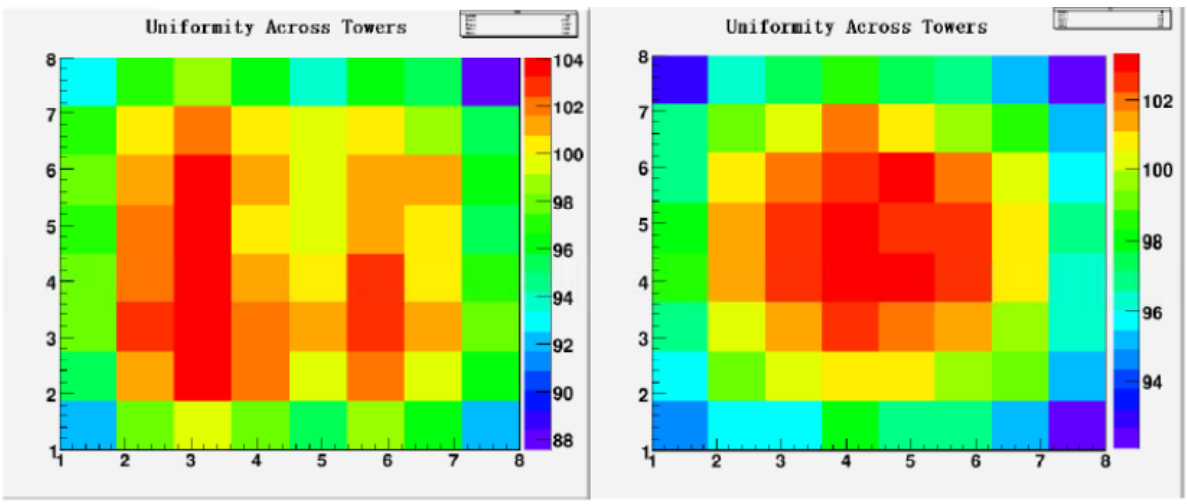

Figure 2.8: Transverse non-uniformity as measured in the test run (left panel), as simulated with GEANT4 (right panel). The X and Y axes are scintillation hodoscope channels. The Z axis is normalized energy deposition in the single super-module.

Figure 2.8 shows the non-uniformity in the SPACAL super-module as measured in the test run and simulated with GEANT4. The transverse leakage and overall skew seen in the data and MC are due to the limited size of the super-module and angular orientation with respect to the beam axis. In the area

indicated in figure 2.8 (hodoscope channels 3-6 in X and Y) where the transverse leakage is small, the non-uniformity as measured in the test run is 1.4% (rms). One can observe a slight difference in the leakage from the sides. This, we believe, is due to the fact that the transverse shower profiles in MC are always narrower than the experimental results. Slightly higher non-uniformities in the experimental data can be explained by the quality of the front face mirror used for the SPACAL.

The committee asked a specific question if the binning of 4.8 x 4.8 mm^2 is sufficient to judge about transverse non-uniformities. In the past, responses of different prototypes of the Sc/Fi calorimeters have been studied with beam scans across the surface (the finest scan was done by the RD1 collaboration with a binning of 2 x 2 mm^2 [5], while the SPACAL collaboration used a grid scan with a binning of 3x3 mm^2 [6]). These studies were performed to measure the transverse non-uniformities and most importantly to determine the constant term in the energy resolution of the detectors which becomes a dominant factor at higher energies. Tracking information was needed to determine if the impact point was at the absorber or at the scintillation fiber, as shown in figure 2.9, below. The origin of the constant term is well understood for fiber calorimeters: the sampling fraction for the early part of the shower depends on the impact point of the particle because of the very small lateral size of the shower in the early part of the shower development. Particles impacting the calorimeter absorber, on average, produce smaller signals than particles entering the fiber. There is also a strong dependence on the incident angle. Measurements by the SPACAL [6] and RD1 collaborations shows that the constant term becomes smaller than 1% for impact angles exceeding 4 degrees as shown in figure 2.11 (note that MC overestimates the constant term).

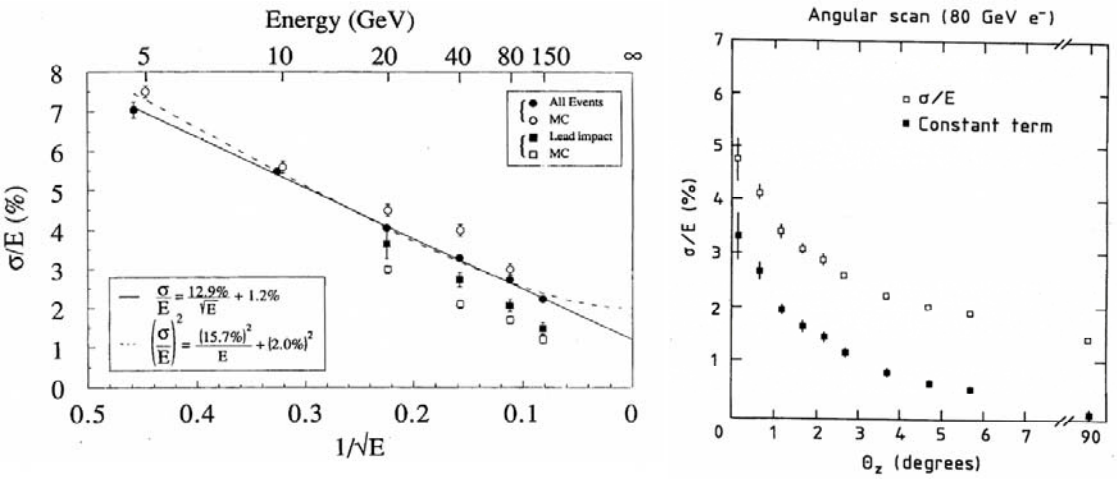

Figure 2.9: Energy resolution of original SPACAL compared with MC for impact points at absorber and Sc fibers (right panel). Dependence of energy resolution and constant term vs incident angle as measured by SPACAL collaboration (left panel).

In the energy range of EIC, resolution of the sampling calorimeters will be dominated by sampling fluctuations. As long as the targeted energy resolution of the detectors is close to 10%/√E, the effects that were usually measured during test runs for HEP experiments at higher energies will not be seen at lower energy beam settings. We performed a MC simulation with an attempt to separate the influence of different instrumental effects on the energy resolution of the W/ScFi (our SPACAL type prototypes). The results are shown below in figure 2.10. For clarity, the energy range is divided into two intervals, one that

was accessible during the test run and more relevant for EIC, and the other which is more relevant for the STAR forward upgrade, but was not accessible for us during the FNAL test run.

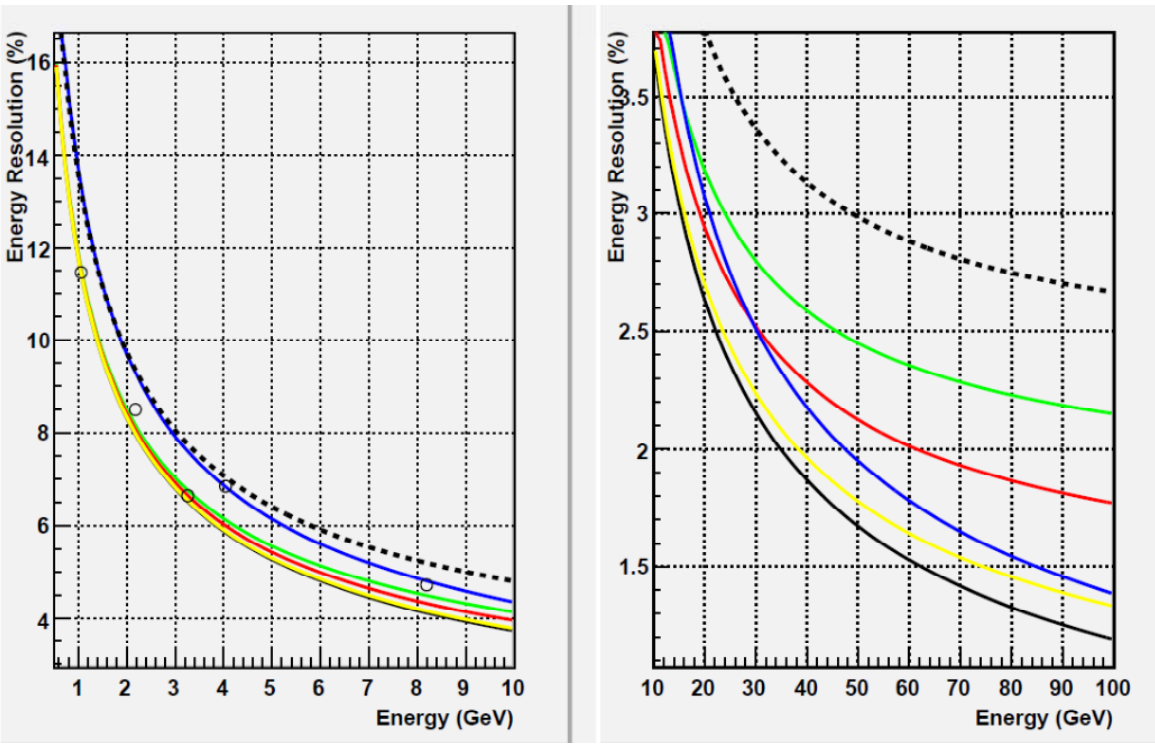

Figure 2.10: Contribution of different factors to the energy resolution of the W/ScFi SPACAL. Black – ideal. Yellow – added constant term due to impact point at fibers or absorber (4 degrees angle, RD1 experimental result, NIM A337), Blue – photo-statistics 200 p.e./GeV, Red – attenuation length 50 cm, Green - non-uniformity of light collection RMS 3 %, Dotted – all of the above, combined. Results are preliminary; tune of GEANT4 parameters will be required. Open circles – our test run T1018 results, corrected for leakage.

The particular choice of parameters in these calculations is explained below. An attenuation length of 50 cm was considered as the worst case scenario of degradation of attenuation length due to radiation damage, even though the attenuation length measured during our test run (derived from the transverse scan with electrons) was ~100 cm. According to measurements by K. Hara et.al NIM A 411 (1998) 31, "Radiation hardness and mechanical durability of KURARAY optical fibers" (the type of fibers used in our prototypes), the attenuation length for these fibers may decrease by factor of two after receiving a dose of about 100 kRad. The effect of the decrease of attenuation length on resolution is very small.

The constant term in the energy resolution was adjusted by hand. For this, we used the experimental results of the RD1 collaboration since their sampling frequency, sampling fraction and diameter of their fibers is close to what we used in our prototypes. Again, at low energies it is practically impossible to measure this term. Non-uniformity of light collection will be explained in the next section. For the purpose of this discussion, this parameter is about twice as large as the value derived from our measurements in the test run.

The most important factor at low energies is photo-statistics. During the test run, we measured 2000 p.e./GeV, however that was achieved using a light collection scheme which was almost 100% efficient. The value of 200 p.e./GeV fed into the MC was chosen after a preliminary investigation of compact SiPM readout for EIC. At present this is the main problem in reaching a final resolution of $10\%/\sqrt{E}$. We find a

requirement of about 500 p.e./GeV to make the contribution of photo-statistics to the energy resolution of current prototypes negligibly small.

To summarize, the most important instrumental effect for EIC sampling calorimeters, assuming the targeted energy resolution is close to 10%/√E, is the efficiency of light collection. That is why we intend to focus our next R&D effort on compact readout with SiPMs.

2.5. Discussion of Compact Readout with SiPMs

During the summer 2012 we looked into a possible scheme of compact readout with SiPMs. Questions of efficiency and uniformity of light collection were investigated by a summer student at UCLA using the setup shown in Figure 2.11.

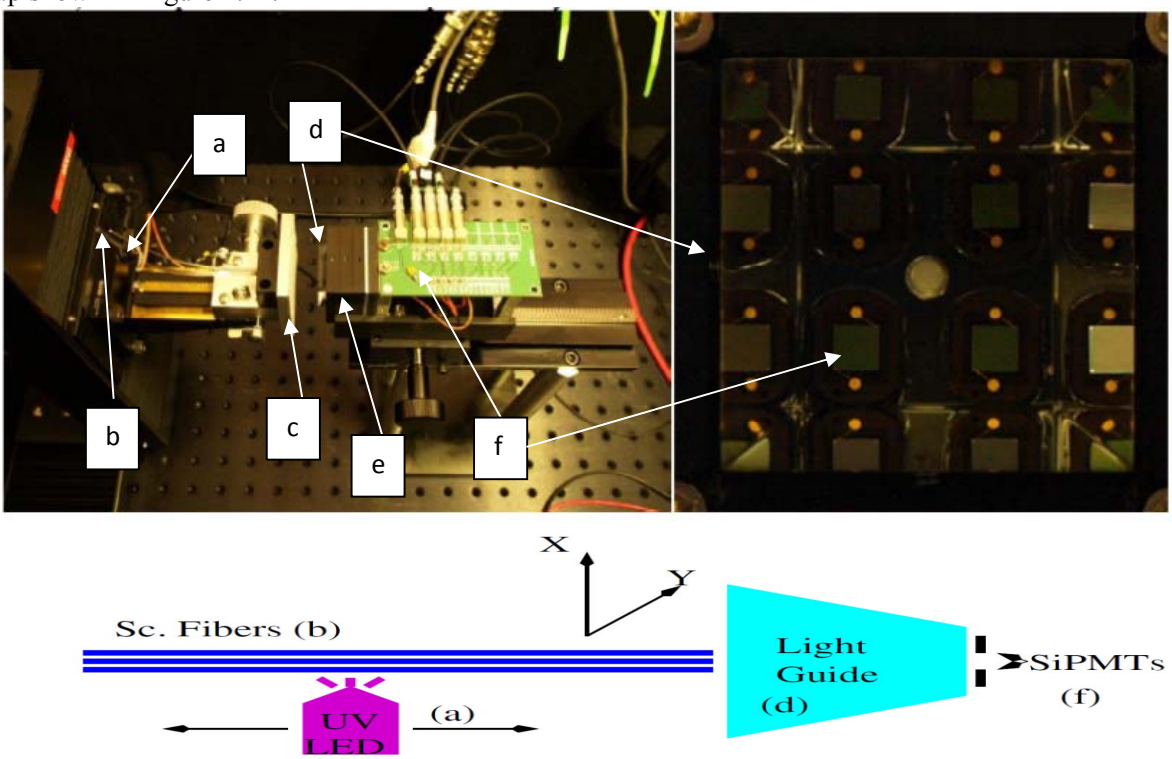

Figure 2.11: Experimental setup to measure light yield and uniformity of light collection (left). View from top of SiPM/Light collector assembly: (a) 350 nm UV LED used to excite scintillation fibers (LED slides along the length of the fibers), (b) bundle of KURARAY blue scintillation fibers, (c) endplate of the light source which can be equipped with ESR film, white diffuser or black tape, (d) the front end of the light guide, (e) holder for light guide (or WLS plates) and SIPMs, (f) distribution board for SiPMs. The front view of light guide (d) is shown in the left panel (light guide in this case has 1” x 1” entrance area, 0.7” x 0.7” exit area, and 0.7” depth) with four SiPMs (f) on the back side (right).

The light source was made from scintillation fibers excited by a 350 nm UV LED (a); the same procedure used by KURARAY to measure the spectra of light in their scintillation fibers. We found that the angular distribution of the intensity of scintillation light depended weakly on the position of the UV LED (fig. 2.11 (a)) along the fibers when the direction of the UV light was perpendicular to the fiber axis. However, if the same fibers were excited from the tip of the fibers (b), with the axis of the LED aligned with the axis of the fibers, the small fraction of direct, long wave light from the LED can significantly

affect the results. For that reason most of the measurements at the end were made with the LED positioned along the fibers, at approximately the position of the "shower maximum" for electromagnetic showers.

A precision 2D mapper was used to move the light source across the surface of the light collection elements. The distance between the light source endplate (c) and light collection elements (d) during scans were kept at 100 μm.

As different light collection elements, labeled (d) in figure 2.11, we tested rectangular WLS plates and two types of acrylic light guides. The WLS plates had different edge treatments, either polished or painted white. The back and front sides of the WLS plates were faced with ESR film, white diffuser film or with black tape. Acrylic light guides were polished and no wrapping was used on the edges.

The entrance area of the light collection element was usually 2.54 x 2.54 cm^2. Four SENSL 3x3 mm^2 SiPMs were usually used for readout. The position of the SiPMs can be easily changed. Each SiPMs was read out independently. SiPMs were optically coupled to the light collection element. For absolute calibration we used the same PMT, previously calibrated for the test run, to measure absolute light yield from the prototypes.

Preliminary findings are: a good uniformity of light collection with WLS plates probably can not be achieved, because direct light from the fibers under the sensors creates hot spots in the response which is twice as large as that at the edges. "Dimpled" schemes for light collection with WLS plates were not tested, because they were likely to make things worse. Such schemes were reported for detecting MIPs in scintillation tiles by CALICE etc., but these are different cases. Short light guides are the most promising way to go in the future. Use of a light guide will also simplify the optical-mechanical-electrical and monitoring integration at the end of the towers.

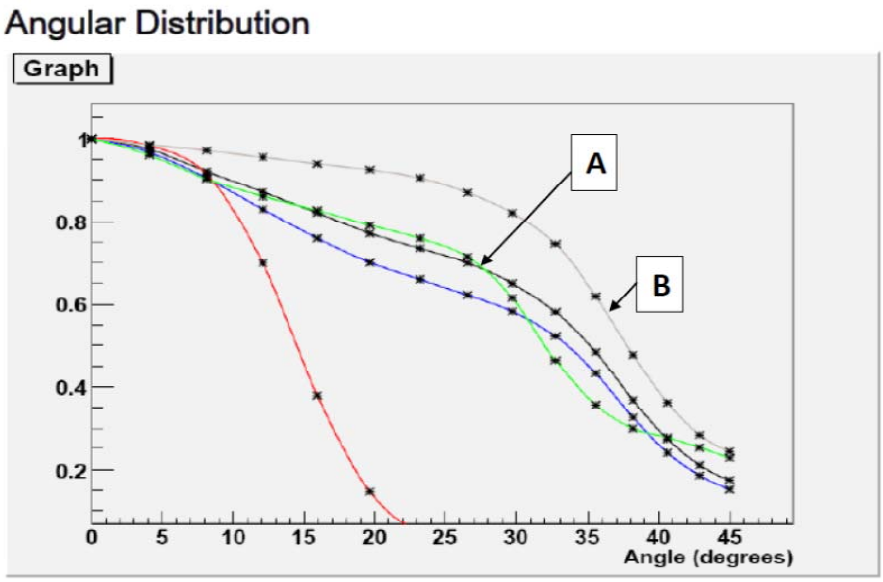

Figure 2.12: Angular distribution of light intensity from the scintillating fiber bundle for different configurations of light source. (A) Distribution for single-clad KURARAY fibers. (B) Distribution which is likely close to multi-clad fibers. Other curves were obtained with a HAMAMATSU picosecond laser (red) and with fibers being excited from the tip (blue/black) which are not relevant to a realistic detector geometry.

The uniformity of light collection strongly depends on the angular distribution of light intensity coming from the end of the scintillation fiber bundle. The angular distribution of light depends on the type of fibers, the method of excitation, and how the fibers were arranged in the bundle, in particular, if optical epoxy was used to kill cladding light and if all fibers are parallel to each other. The measured angular distributions of light intensity for the sources used during this summer are shown in figure 2.12.

The green curve marked (A) represents the case of single-clad KURARAY SCSF78 fibers. Angular distribution (B) is closer to the case of multi-clad fibers, however this curve was obtained from single-clad fibers which were twisted into a bundle. We will see below that the resulting uniformity of light collection strongly depends on these distributions.

The resulting scans with WLS plates and a short light guide is shown below in figure 2.13. The bin size in the plots are ~0.9 mm horizontally and ~2 mm vertically.

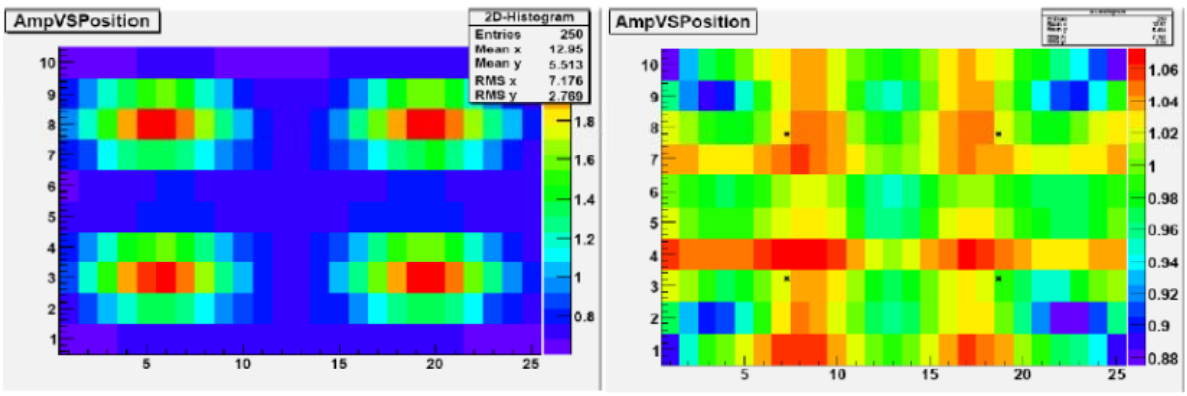

Figure 2.13: Uniformity of light collection with WLS plate (mirror at back side, diffuser at front side, and diffuser at edges) on the left (best test results). Uniformity of light collection with short light guide shown on the right. In both cases, the angular distribution of light intensity is (B) as shown on figure 2.12.

The uniformity of light collection with the light guide shown in figure 2.13 is 3% (rms). When the same configuration of SiPMs and light guide was tested with the light source having angular distribution (A) the uniformity of light collection dropped to ~ 6% (rms). In both cases the efficiency of light collection is about 10%.

After this preliminary investigation of compact readout, we think that for an EIC sampling calorimeter it will be better to use double-clad scintillation fibers. This will improve the uniformity of light collection and bring us closer to the desired 500 p.e./GeV. The use of Hamamatsu MPPCs should help as well because its photon detection efficiency is better than the SENSL device which was used for these scans. For the construction of a barrel EMC prototype we will acquires multi-clad fibers from KURARAY.

2.6 Calibration and Monitoring Considerations

The schemes of absolute calibration for the EIC calorimeters will depend on the scattered lepton kinematics.

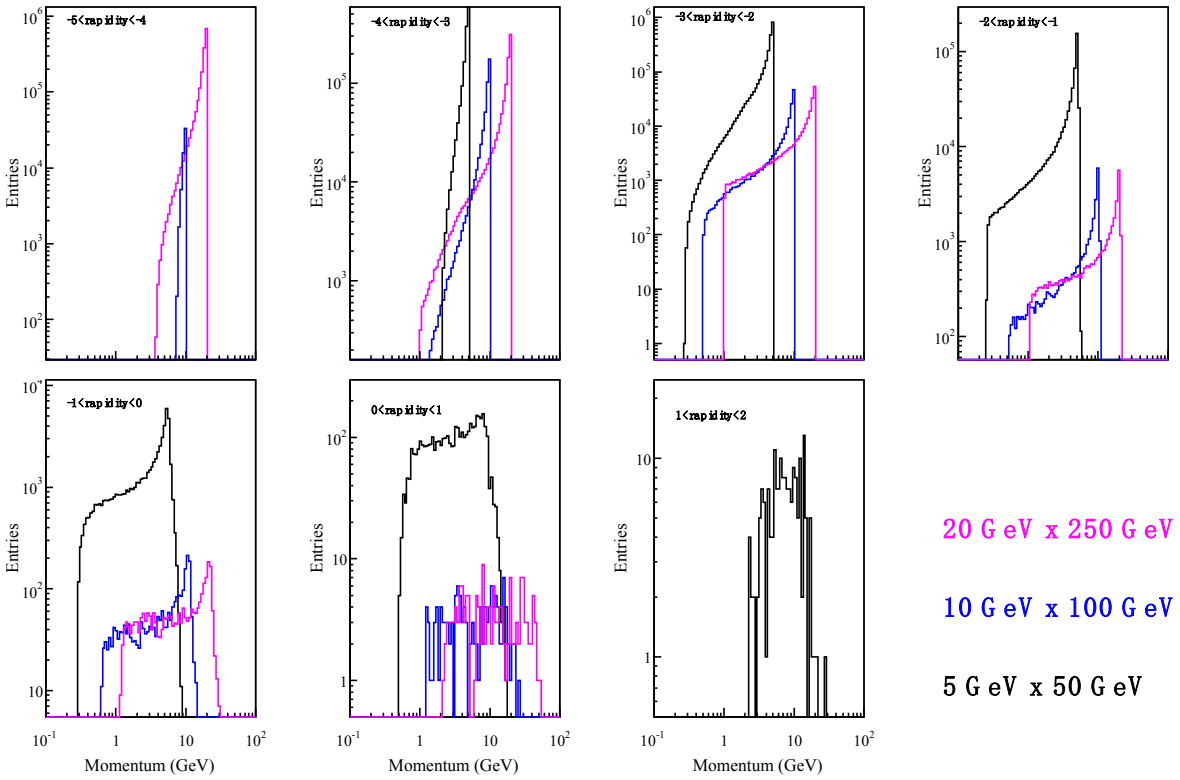

Figure 2.14: Scattered lepton kinematics anticipated for EIC collisions. Momentum distributions are calculated for the scattered lepton for different center-of-mass energies and different rapidity bins in the laboratory frame. The following cuts have been applied $Q^2 > 0.1$ GeV^2, $0.01<y<0.95$ and $-5<\text{rapidity}<+5$.

The most straightforward way to calibrate the sampling EM EIC calorimeters (barrel and forward region outgoing hadrons) is to use tracker information. For example, at the lowest $\sqrt{s}$ (5x50 GeV), the momentum of the electrons in the barrel region will be precisely measured by the tracking system which allows an absolute calibration of the calorimeter on a tower-by-tower basis. The absolute scale for the endcap calorimeters can be set with electrons, but a tower-by-tower calibration will most likely be done with π^0s and MIPs. These are typical schemes for general purpose collider detectors, such as STAR, for example. Initial calibrations with test beams can be done with electrons and MIPs. One implication of such schemes is the requirement on noise and dynamic range for electronics, as well as absolute light yield from the detector. For example, the requirement to use the MIP peak for absolute calibration may be the most stringent requirement on light yield (not the photo-statistic contribution to energy resolution discussed above). These questions will require detailed investigations which can only be done with a more realistic reference detector geometry. These requirements must be kept in mind during R&D, particularly with regards to limitations imposed by compact readout and light collection efficiency.

Given the level of radiation exposure for EIC sampling calorimeters as discussed above, we don't anticipate any significant secular change in the response of the scintillation fibers. There are no other known factors which can lead to rapid changes in the response of plastic scintillators for an EIC detector. Unlike LHC experiments where monitoring corrections for crystals have to be made on a fill-by-fill basis,

with the rate of radiation exposure at EIC these rates are negligibly small. Thus, the monitoring scheme can be a simple LED or laser monitoring system to track the response of the SiPMs. Any long-term changes in the properties of the scintillation materials can be tracked globally (barrel and end caps eta rings) by E/p, mass shift etc.

2.7 R&D on Light Collection, Compact Readout and Barrel EMC Prototype

The next major goal of our R&D project is to achieve optimal light collection with compact readout. One possible method to do compact optical-mechanical-electrical-monitoring integration for W/ScFi-type calorimeters is shown below.

The last brass mesh shown in figure 2.15 will be mirrored. This mesh will reflect a portion of the light from a single monitoring fiber into the four towers of the super-module. A small interface board with four SiPMs will be attached directly to the light guide. An external cover snaps on to provide an interface for the monitoring fiber and the rest of the FFE, including the bias for the SiPMs. We will investigate compact readout schemes during construction of the barrel EMC prototype. For this stage of R&D we want to understand what level of compensation of the gain drift of SiPMs with temperature can be achieved. If thermo-stabilization is required, we will investigate what level of monitoring will be required and what can be reached with the compact readout scheme. Technology limitations need to be understood, but global requirements which can come only from extensive simulations with the reference detector have to be formulated as well.

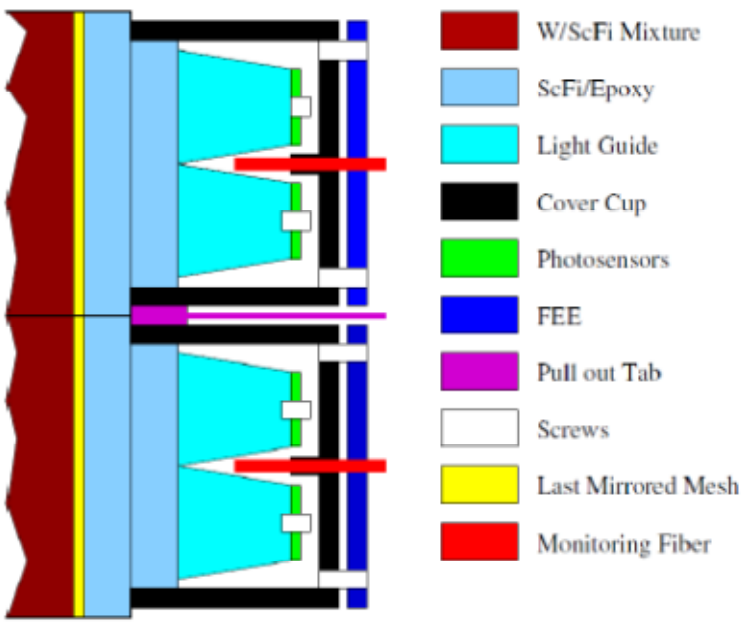

Figure 2.15: Possible scheme of optical-mechanical-electrical and monitoring integration for W/ScFI type calorimeters (not to scale, the length of the "readout part" will depend primarily on compactness of light guides).

Calorimeters in the EIC main detector are naturally divided into three regions; outgoing lepton (A), outgoing hadron (B), central barrel calorimeter (C). Ideally, a calorimeter system should combine a finely-granulated electromagnetic section with a very good hadronic calorimeter (combined strength of both H1 and ZEUS detectors at HERA, in one detector at EIC), because the kinematics variables important for DIS (Q^2, x, y) are obtained by measuring the momentum and/or hadronic energy and the direction of the scattered lepton and/or the hadronic energy. The redundancy in the determination of the kinematic variables is a crucial point and presents many advantages: minimization of the migration between the 'true' and the measured kinematic variables by choosing one particular method; cross calibration of the various calorimeter devices, and studies of photon radiation from the lepton line by comparing leptonic and hadronic information [7]. Unlike at HERA, with two independent experiments, the EIC envisions only one dedicated detector, which makes such redundancy even more important.

Each of the three calorimeter regions will have its own challenges. As it seen now, the most important are for (A); a very high energy resolution to measure scattered electrons (at ~1% level). That should be combined with small Moliere radius and high granularity to distinguish closely-spaced clusters at distance of less than 2 cm. Thus, heavy crystals are the only solution for this. Energy resolution at the 1% level is a real challenge.

For the central region, the requirements are less clear, in part, because in this region the expectation is that the tracking detector will perform very well. Hermeticity will be required, as well as compactness. Compactness will have big impact on the cost of the detector. Energy resolution at the level of $\sim 10/\sqrt{E}$ seems to be sufficient. Compensation to achieve best possible energy resolution for single hadrons (with a possibility to add a barrel hadron calorimeter later) is not an obvious requirement. Again, this will depend on tracker performance. Granularity and projectivity are also not yet well-studied. The average multiplicity in ep collisions is very low (~8). It is quite possible a barrel EMC could perform well in a non-projective configuration. If so, that will enormously simplify the design and drive down the cost.

For any technology being used in the central region, hermeticity and compactness are challenging requirements. There have been no ScFi barrel calorimeters build in the past with a traditional 'tower' configuration layout. The goal of R&D in Year Two is to extend the W powder Sc/Fi technique to build wedge-type towers, develop compact readout, and verify with a test beam that the targeted energy resolution of $\sim 10\%/\sqrt{E}$ has been achieved. This R&D should give us a good idea of the limitations of the W/ScFi technique for applications in the central region. At the same time, questions of projectivity and granularity will be investigated with MC using a model of the calorimeter with detector parameters, composition and resolution close to those achieved during Year One of this R&D. The details of how that should be done are presently under discussion.

For region (B) we assumed that at start up, both the EM and HAD sections will be in place. In this region requirements primarily will be driven by the best possible reconstruction of hadronic energy and direction of energy flow, where a highly granulated and compensated calorimeter system is the best solution. A somewhat similar R&D program will be investigated for the STAR Forward Upgrade, where the EM section will be built using the same techniques we developed in Year One of R&D for EIC, and the hadronic section will be a traditional sampling Pb/Sc tile calorimeter (10 mm Pb /2.5 mm Sc). Because of the obvious similarities of the systems and overlap of manpower involved in both the STAR and the EIC R&D efforts, we are not requesting any EIC funds at this time to do hardware development for region (B).

In the EIC detector model we plan to implement a binary (EM+HAD) configuration, similar to that used by STAR, as a first step to look at detector performance for EIC.

2.8 Division of Responsibilities

Groups involved in Year One or R&D (UCLA/TAMU/PSU) will be primarily responsible for developing technology and building a matrix of 3x5 wedge-type towers (tower size 1”x1”x18 X0), as well as to investigate schemes for compact light collection using SiPMs. A barrel EMC prototype of this size will allow us to measure the response of the detector with impact angles up to 45 degrees (which covers the central detector). A visiting post-doc at UCLA will help with the construction of the prototype, will continue our MC investigation of instrumental effects and will help to build the GEANT model for a barrel EMC detector within the EIC detector configuration, in close collaboration with the BNL group.

Groups from BNL and IUCF will be responsible for investigating the tungsten-scintillating fiber accordion calorimeter design and to developing a readout system for the MPPCs (preamps, bias, and thermo-compensation), thus the request to support an electronic engineer from IUCF in our budget. Undergraduate students from participating universities will be involved in characterization of the MPPC (PDE, temperature-dependence, etc.). They will also help with the construction of the prototype, bench testing, etc.

The BNL group will also play a leading role in simulations, with help from all other groups.

We expect to carry out a test run in late 2013. All groups are expected to contribute to the beam test run. We will most likely use the test facility at SLAC, where beam conditions are most favorable for EIC calorimeter R&D, however, other facilities such as FNAL and DESY are also under consideration.

2.9 Budget Update and Timescale

Photo-detectors and associated electronics	$14k
Machine Shop	$10k
Student Labor (includes 26% overhead)	$12.6k
Visiting Post Doc (includes 26% overhead)	$31.5k
Electronics Engineer (includes 56% overhead)	$27.3k
Supplies for prototype (fibers, meshes, epoxy etc.)	$12k
Test beam (travel, shipping, includes 26% overhead)	$15.1k
Total direct cost	$100.5k
Total indirect cost	$22k
Total	$122.5k

References

[1] Groom, D. E. *et al.,* Nucl. Instr. and Meth. **A279**, 1

[2] Stevenson, G. R., "New Dose Calculations for LHC Detectors", Proc. ECFA Large Hadron Collider Workshop, Aachen, Oct. 1990, CERN 90-10, ECFA 90-133, vol. II, p.566

[3] Acosta, D. *et al.*, Nucl. Instr. and Meth. **B62**, 116

[4] Anderson, J., "Upgrade of the CMS Hadron Calorimeter for Upgraded LHC", CALOR 2012

[5] Badier, J. *et al.*, Nucl. Instr. and Meth. **A337**, 314

[6] Acosta D *et al.* 1991, Nucl. Instr. and Meth. **A308**, 481

[7] Zomer, F., "Inclusive Deep Inelastic Scattering at HERA and Related Phenomenology", arXiv:hep-ph/9912441v2

3) Progress Report on the Tungsten Scintillating Fiber Accordion Calorimeter Development and Readout Electronics

The BNL Group has been pursuing an alternative approach to a W-SciFi calorimeter that is based on a so-called optical accordion design. This design was described in our previous R&D proposal that was submitted in April 2012 and approved for first year funding in May 2012. We describe here the progress made on this design since last Spring, along with progress on the development of the readout electronics that will be used for this calorimeter and/or for the W-Powder/SciFi SPACAL design described above.

Our focus over the past six months has been in three main areas: 1) study the fabrication of the tungsten scintillating fiber "sandwiches" that form the basic structure of the optical accordion, 2) study the light output from the fibers after assembly into the sandwiches and collection of the light onto the SiPM readout device, 3) development of the readout electronics for the SiPM, including the preamp and the temperature monitoring and control system for adjusting the bias voltage to minimize gain variations with temperature. We briefly describe below the progress in each of these areas.

3.1 Fabrication of the Sandwiches

The sandwiches consist of a layer of scintillating fibers that is sandwiched between two tungsten metal sheets that have an accordion shape and are glued together with a tungsten powder epoxy (similar to the W-powder epoxy used in the SPACAL design). These sandwiches have a wedge shaped structure that allows them to be formed into a ring that has a projective geometry that points back to the interaction vertex, and can have their fibers arranged in such a way that they are also approximately projective along the beam direction.

We have been working with a company (Tungsten Heavy Powder in San Diego, CA) to produce these sandwiches, with the goal of developing the technology to fabricate large (> 1 m in length) complete components of the final calorimeter in industry. We have constructed a number of small prototype sandwich modules, such as the one shown in Fig. 3.1, that has allowed THP to develop the tooling and assembly techniques for producing the sandwiches, and allowed us to study their properties, such as their light output and mechanical characteristics.

A number of issues related to the construction of the sandwiches were studied during the past several months. These include:

- Develop the tooling needed to bend the accordion plates
- Study the mechanical characteristics of the resulting accordion plates and develop techniques for minimizing distortions and spring back (including studies to optimize the plate thickness used for each sampling layer)
- Develop a procedure for laying out the fibers and positioning them inside the sandwich
- Develop the tooling for constructing the wedge shaped layer of fibers and tungsten powder epoxy that forms the center of the sandwich, and then constructing the wedges.

- Finding a glue that has a minimal effect on the light output of the fibers yet provides enough mechanical strength to hold the assembly together

Figure 3.1: Single layer accordion sandwich consisting of two 1 mm thick metal plates with a layer of 1 mm scintillating fiber and tungsten powder epoxy in between. Fibers are left protruding in order to perform light output measurements. They will be cut flush with the absorber plates in the final calorimeter. Although it is not apparent from the photo, the sandwich has a wedge shaped structure along its length, varying in thickness from 3.13 mm at the front to 3.36 mm at the back.

As a result of these studies, we are now also exploring a new approach of making a wedge-shaped absorber plate and gluing a uniform thickness layer of scintillating fibers in between. This has the advantage that the fabrication of the absorber, which would include the tungsten metal plates and tungsten powder epoxy, could be constructed without interacting with the scintillator, allowing more possibilities for heating, various types of glue etc., and then the scintillating fiber layer could simply be glued in between the resulting plates.

3.2 Light Output from Fibers and Light Collection onto a SiPM

We have studied many types of scintillating fibers (Saint-Gobain BCF12, BCF60, Kuraray SCFS-78, round, square, single clad, and multiclad) in combination with various types of glues in order to determine the effect of the glue on their light output. We have found certain types of glue affect the light output more than others, and that the type of cladding also affects the light output in the presence of the glue. Figure 3.2 shows a summary of some of these measurements.

The results shown in Fig. 3.2 are typical of those with different types of fibers and glues, but other glues were found that have more or less of an effect on the light output. However, one conclusion that can be drawn from all such studies is that multi-clad fibers are less affected by the glue than single clad fibers. This is expected since the glue mainly affects the cladding light trapped in the fiber has less of an effect with a second layer of cladding. The other conclusion is that there is still a fairly steep position dependence near the readout end of the fiber even with the glue. It may therefore be necessary to take additional steps to flatten the attenuation curve of the fibers in order to improve the energy resolution.

As stated earlier in this proposal, it is very important to have sufficient light output from the fibers and to collect this light onto the SiPM (or group of SiPMs) in order to achieve adequate photostatistics so as not to adversely affect the energy resolution of the calorimeter. We have therefore studied various

methods to collect the light from the bundle of fibers that would comprise a single tower of the calorimeter onto a single SiPM to see what the limits in uniformity and light collection efficiency would be. We tested a light collector consisting of a wavelength shifting block, similar to the one described in Section 2.5, and came to the same conclusion, namely, that due to the component of direct light reaching the SiPM, it would not be possible to achieve good uniformity in the overall light collection using this method. We then studied a small lucite block (similar to the light guide configuration described in Section 2.5) and achieved much better results with a single SiPM mounted onto the side of the block.

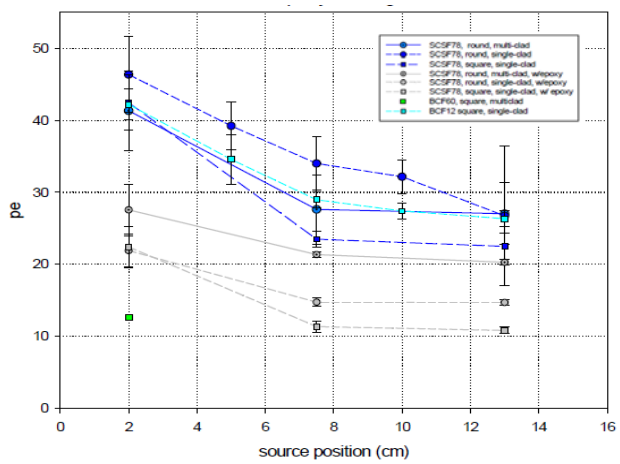

Figure 3.2: Light output from various types of scintillating fibers with and without embedding in one particular epoxy studied (WC748). Other epoxies where shown to have more or less of an effect. Measurements were made with a Hamamatsu S10362-33-25C MPPC and the light yield was converted to the number of photoelectrons detected.

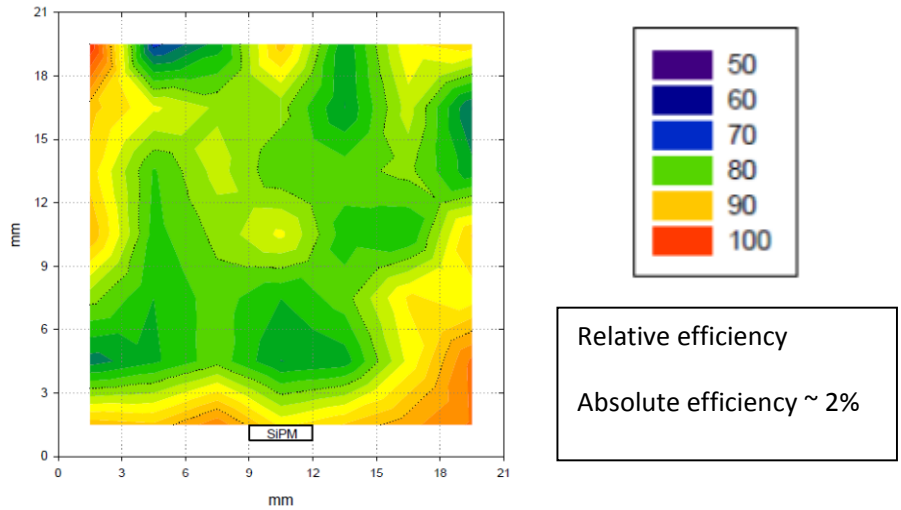

Figure 3.3: Uniformity of light collection using a 21x21x19 mm lucite block read out with a single SiPM (Hamamatsu S10362-33-25C MPPC) centered on a 21x19 mm surface. The block was covered in white teflon on 5 sides and the side containing the fibers had white reflector between the fibers. No coupling was used between the fibers and the block.

Fig. 3.3 shows the results of one of these measurements. The uniformity across the block is ~ 20 % and the overall collection efficiency was found to be ~ 2%. There was also no significant enhancement of the response immediately in front of the SiPM. While the overall uniformity and light collection efficiency is lower than was found for the 4 SiPM readout in Section 2.5, the results indicate that a light guide method for collecting the light is better than the use of a wavelength shifter. It also illustrates the tradeoff between having better uniformity and light collection efficiency versus the higher cost of implementing additional SiPMs in the readout. We intend to further study this method, as well as various other methods of collecting the light from the fibers, with both single and multiple SiPM readout during the next phase of our R&D.

3.3 Readout Electronics and Temperature Monitoring and Control

We have designed and built a prototype circuit for reading out the SiPMs from either the SPACAL version or the accordion version of the calorimeter. It contains a preamp and a temperature monitoring and control circuit for each SiPM that provides an adjustment to the bias voltage which compensates for the change in gain as a function of temperature. A block diagram for this circuit is shown in Fig. 3.4, along with a first single channel prototype board. The circuit contains a thermistor, control logic and a 10 bit DAC for adjusting the bias voltage, and the output drives a differential line to a separate ADC located downstream in the readout chain. A new 16 channel prototype board has just recently been completed and is currently being tested.

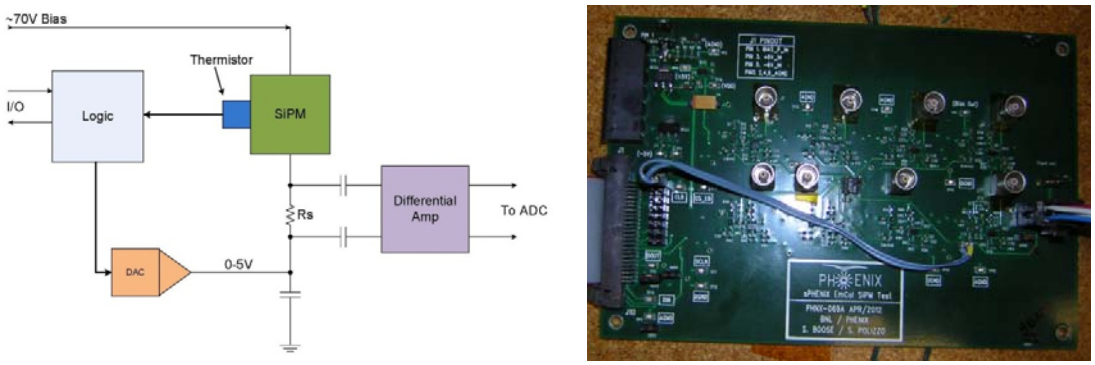

Figure 3.4: Block diagram for the prototype preamp and temperature monitoring and control circuit for reading out the SiPMs from the calorimeter (Left), and a first version of the preamp and temperature monitoring and control board (Right)

3.4 Future plans

Development of the technology for producing the accordion sandwiches will continue in collaboration with Tungsten Heavy Powder over the next several months which will lead to a choice for the method for producing the sandwiches for a first prototype accordion calorimeter module. This module will consist of approximately 5x5 towers, each ~ 2x2 cm^2, that will be tested first with cosmic rays and later in a test beam along with the SPACAL calorimeter. In parallel, we will continue to study the light output from the fibers and various light collection schemes for collecting the light with good uniformity and efficiency

onto one or more SiPMs. The prototype readout electronics will be used to read out the SiPMs and study the ability to measure their temperature and control their gain. An overall optimization of the light collection scheme and readout electronics will then be used for calorimeter prototype. No additional funds are requested at this time to carry out these studies, and further details will be provided during the next Committee Review.

4) Progress Report on the Crystal Calorimeter R&D Project

4.1 Initial Preparation

In our laboratory at the USTC (University of Science and Technology of China) a system for the testing of crystal light yield output and decay time has been built. Some photographs and schematic diagrams of the test system are shown below.

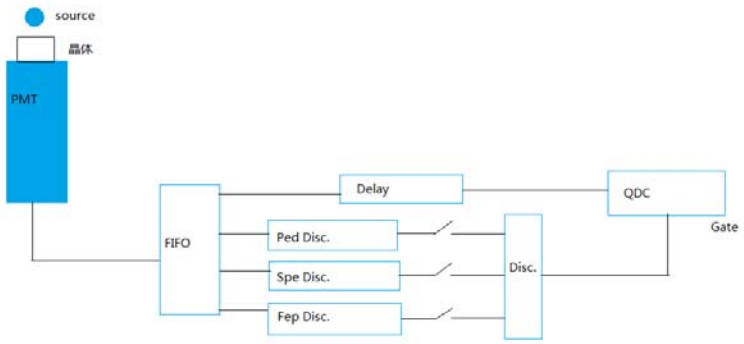

Figure 4.1: Schematic diagram of the USTC test system.

Figure 4.2: Left: Dark box with crystals and PMTs sealed inside. Right: QDC

Figure 4.3: Left: VME crates. Right: Computer with Labview control and oscilloscope.

Our vendor SICCAS (Shanghai Institute of Ceramics, Chinese Academy of Science) produced some small crystal samples for initial testing. The crystals we tested are labeled as:

- PWO-A 30×30×45 mm
- PWO-B 25×25×220 mm
- BSO_S 25×30 mm
- BSOL 20×20×200 mm

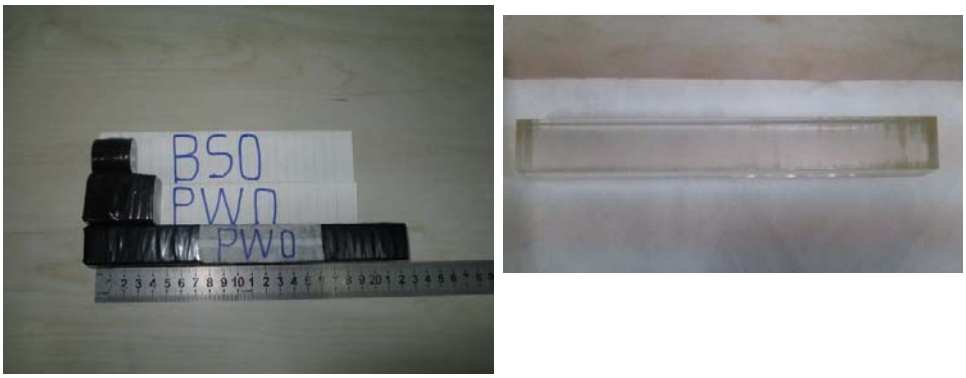

Figure 4.4: Left: PWO crystals and short BSO crystal wrapped with black insulation tape. Right: BSO_L (20×20×200 mm) crystal recently produced.

By September 2012, SICCAS successfully produced a 200 mm long BSO crystal, but the transmission and purity are not good, especially near the ends of the crystal. The viscosity of the melted BSO under high temperature is much larger than PWO or other crystals. Its purification is very sensitive to the temperature control. The whole Bridgman-Stockbarger process is very slow, usually taking a month to produce a 20×20×200 mm BSO crystal. SICCAS is still developing production techniques, especially with regard to the temperature control.

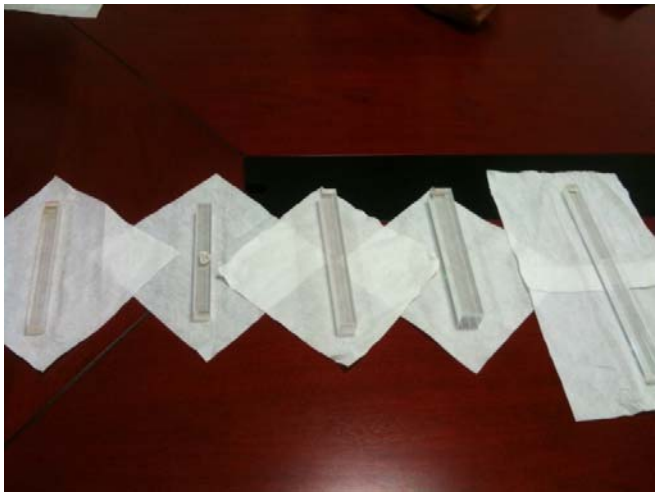

Figure 4.5: From left to right is the BSO_L crystal, PWO crystals with different sizes and a 300 mm long BGO crystal produced by SICCAS.

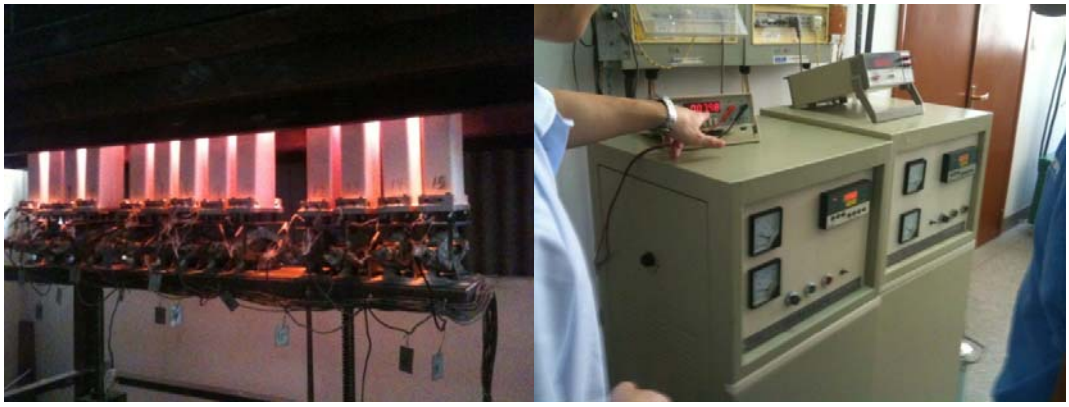

Figure 4.6: Left: Bridgman-Stockbarger production, can produce up to 16 pieces of crystals at the same time. Right: Temperature control system.

4.2 Crystal Testing Results

We obtained the BSO and PWO emission spectra using 1 cm^3 cubes which were cut from the BSO/PWO seed crystals from the Material Structure Center in our University. Below are the emission spectra.

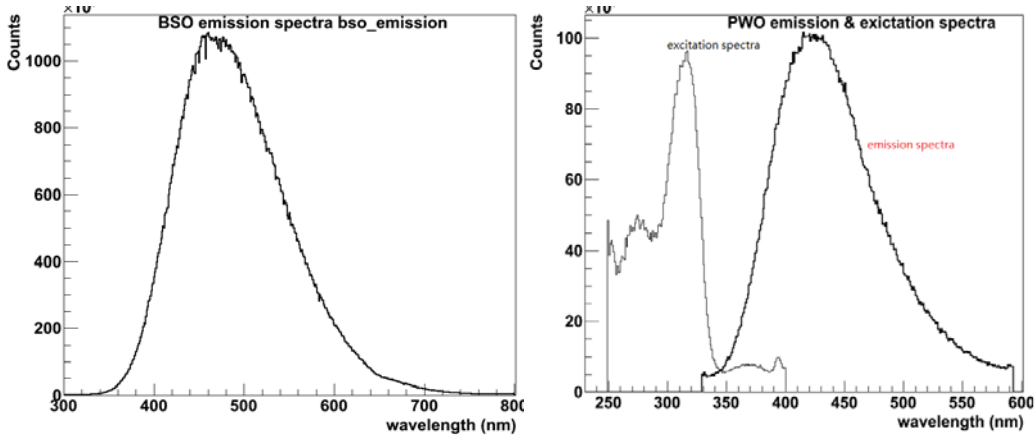

Figure 4.7: Left: BSO emission spectra. Right: PWO emission and excitation spectra.

The table below summarizes the light yield output for the crystal samples (p.e./MeV):

Source	BSO_L	BSO_S	PWO-A	PWO-B
	20×20×200 (mm)	25×30	30×30×45	25×25×220
Cs-137	34.5	66.6	8.54	24.0
Co-60			10.5	

The results of timing structure tested at room temperature (+25 °C) are compared with the Panda-PWO results at different temperatures (-25 °C - +25 °C), as shown below:

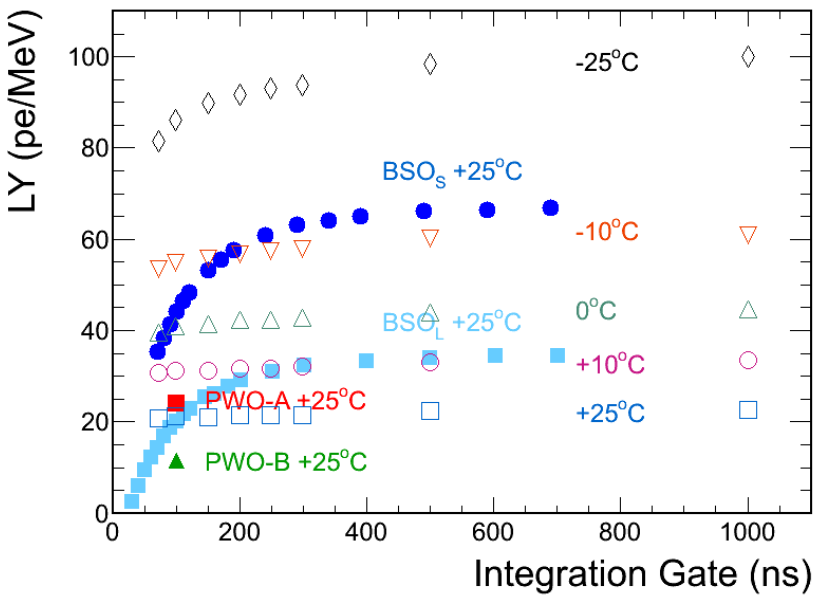

Figure 4.8: Light yield out-put *vs* gate width.

Impurity levels affect the light yield output very much, especially for BSO_L. BSO_S is not as sensitive and is comparable with PWO at -10 °C. This will be improved as SICCAS makes progress in BSO production techniques. If BSO characteristics at room temperature can be made comparable to PWO at low temperature, we can save the cost of the cooling the crystals.

We can also obtain the decay time information for the BSO crystals as shown in Fig. 4.9. We used two components (fast and slow) to fit the data. Impurities may also affect the timing information, but the results are quite close to the published average value of 100 ns.

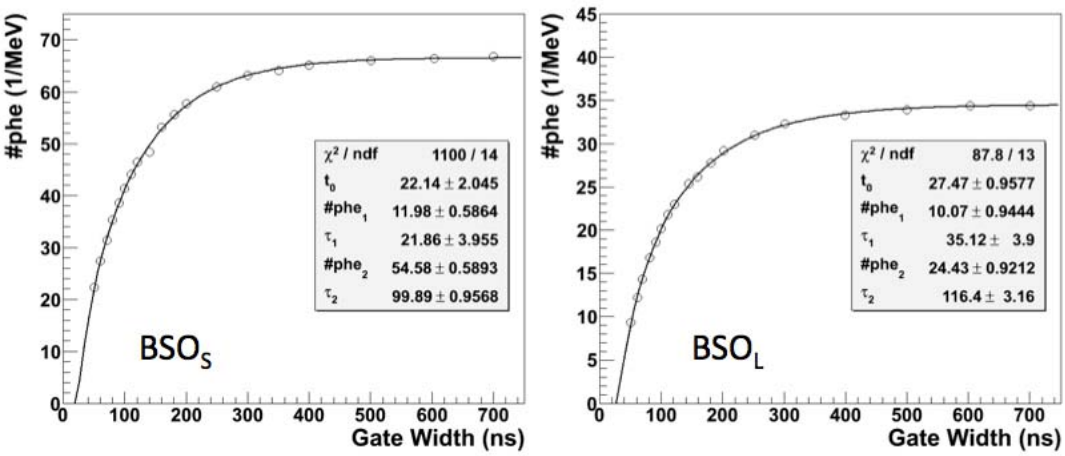

Figure 4.9: Decay time results for BSO crystals.

The table below summarizes the decay time of the BSO crystal samples:

Components	BSO_S	BSO_L
1 (ns)	21.9 ± 4.0	35.1 ± 3.9
2 (ns)	99.9 ± 1.0	116.4 ± 3.2

To study the uniformity of the crystals, we attached a PMT to one side of the crystal(d=0) and move the radiation source to scan different positions along the length of the crystal. The results are shown in figure 4.10. We can see the impurity affects BSO_L significantly at large d.

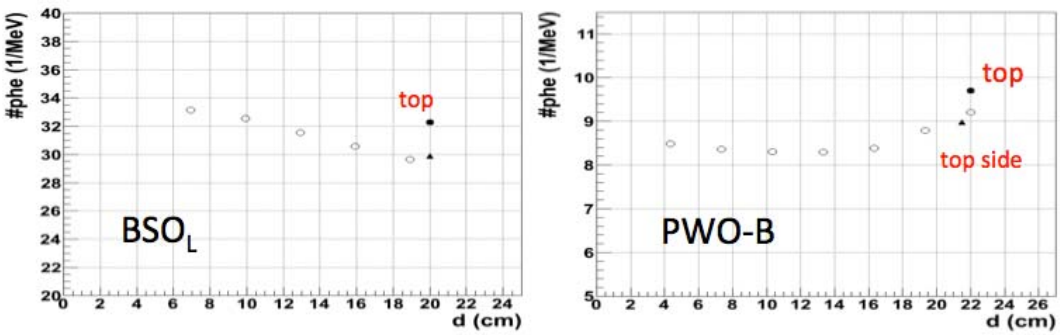

Figure 4.10: Uniformity test results for BSO and PWO crystals.

Currently due to lack of manpower, there is not much progress on simulations. This shortfall will be addressed in the near future.

4.3 Near Future Plan

Our plans in near future (November 2012 - February 2013):

1) Test improved BSO crystals (depend on the progress at SICCAS in crystal fabrication).
2) Design PMT based read-out for a 3×3 or 4×4 BSO crystal array prototype.
3) Possible beam test for the prototype.
4) Continue simulations for design optimization of a crystal calorimeter in an EIC detector.

The critical issue is the reliability of the improved BSO production technique. Our schedule strongly depends on BSO production from SICCAS.